

# A Class of Axis–Angle Attitude Control Laws for Rotational Systems

Francisco M. F. R. Gonçalves, Ryan M. Bena, and Néstor O. Pérez-Arcibia

**Abstract**—We introduce a new class of attitude control laws for rotational systems, which generalizes the use of the Euler axis–angle representation beyond quaternion-based formulations. Using basic Lyapunov’s stability theory and the notion of extended  $\mathcal{K}_\infty$  functions, we developed a method for determining and enforcing the global asymptotic stability of the single fixed point of the resulting closed-loop (CL) scheme. In contrast with traditional quaternion-based methods, the proposed generalized axis–angle approach enables greater flexibility in the design of the control law, which is of great utility when employed in combination with a switching scheme whose transition state depends on the angular velocity of the controlled rotational system. Through simulation and real-time experimental results, we demonstrate the effectiveness of the proposed approach. According to the recorded data, in the execution of high-speed tumble-recovery maneuvers, the new method consistently achieves shorter stabilization times and requires lower control effort relative to those corresponding to the quaternion-based and geometric-control methods used as benchmarks.

**Index Terms**—Axis–Angle, Attitude Control, Robotics.

## I. INTRODUCTION

NUMEROUS different types of attitude controllers have been thus far proposed for stabilizing and commanding the trajectory of rotational systems that can be modeled as rigid bodies [1]–[16]. These controllers can be classified into three main types: (i) quaternion-based, (ii) Euler-angles–based, and (iii) rotation-matrix–based (geometric). The limitations of attitude controllers based on Euler angles have been extensively studied and discussed in the technical literature—for example, see [17] and references therein. For this reason, quaternion-based and geometric methods have been the preferred choices for implementing robust high-performance attitude controllers. Although these two attitude representations implicitly contain the knowledge about the Euler axis and associated rotation angle as defined in [18], this information is generally not directly used in the design of attitude controllers.

For example, quaternion-based time-invariant attitude control laws, usually include a proportional term that is formed

This work was supported in part by the Washington State University (WSU) Foundation and the Palouse Club through a Cougar Cage Award to N.O. Pérez-Arcibia and in part by the WSU Voiland College of Engineering and Architecture through a start-up package to N.O. Pérez-Arcibia.

F. M. F. R. Gonçalves and R. M. Bena contributed equally to this work. F. M. F. R. Gonçalves and N. O. Pérez-Arcibia are with the School of Mechanical and Materials Engineering, Washington State University (WSU), Pullman, WA 99164-2920, USA. R. M. Bena is with the Department of Mechanical and Civil Engineering, California Institute of Technology, Pasadena, CA 91125-2100, USA. Corresponding authors’ email: francisco.goncalves@wsu.edu (F. M. F. R. G.); n.perezarcibia@wsu.edu (N. O. P.-A.).

by scaling the attitude-error Euler axis with  $\sin \frac{\Theta_e}{2}$ , where  $\Theta_e$  is the corresponding instantaneous rotation error. However, there is not a reason for this type of formulation other than ensure continuity in the entire rotational space and simplify the analysis of the resulting *closed-loop* (CL) system. Counterintuitively, however, in most practical applications, this continuous control law is modified to obtain a switching or hybrid scheme to avoid unwinding behavior [4]–[8]. Another consequence of implementing continuous quaternion-based control laws is that, for rotational errors larger than  $\pi$  rad, the proportional-control effort decreases as the rotational error about the attitude-error Euler axis increases. In a similar fashion, geometric-based attitude control laws implicitly apply torques in the direction of the shorter rotational trajectory required to eliminate the attitude error. As discussed in [1] and [2], this direction choice is not necessarily the best for every kinematic situation, depending on the specific performance objectives of the problem of interest.

In this letter, we introduce a class of attitude control laws applicable to a wide gamut of rotational systems that can be modeled as rigid bodies moving in the *three-dimensional* (3D) space, including *uncrewed aerial vehicles* (UAVs), satellites, and microrobotic swimmers. The proposed method generalizes the use of the Euler axis–angle representation in the formulation of the feedback law that stabilizes and drives the rotational motion of the controlled system. It is widely known that global asymptotic stability in the 3D rotational space cannot be achieved with the use of continuous time-invariant feedback controllers. Nonetheless, a common technique used to overcome this topological obstruction is to design discontinuous control laws [8]. Following this approach, by combining Lyapunov’s stability theory and the notion of extended  $\mathcal{K}_\infty$  functions, we developed a method that ensures the existence of a unique CL fixed *attitude-error quaternion* (AEQ) and the global asymptotic stability of the corresponding equilibrium point, which depends on a positive-definiteness condition that the controller gains must satisfy.

A main contribution of the work presented in this letter is the design flexibility enabled by a generalized formulation of the proportional term in the proposed control law; specifically, it allows the user to select a suitable proportional control function based on the platform and/or application, with stability guarantees. Furthermore, in contrast to existing quaternion-based control methods, the new generalized axis–angle attitude control approach ensures a greater proportional action the farther away the system’s state is from the stable CL equilibrium AEQ. This characteristic is especially useful when a scheme of the proposed type is employed in combination with intelligent switching methods capable

of taking into account the angular velocity when selecting the direction in which the input torque is applied during operation, as for example done in the case presented in [1]. We tested the functionality and performance of the introduced approach through simulations and outdoor flight tests. The obtained simulation and experimental data show that compared to two other high-performance benchmark controllers—one quaternion-based and another geometric—a scheme of the new type is unequivocally superior. Specifically, data obtained through dozens of high-speed tumble-recovery maneuvers show that the new approach consistently achieves shorter stabilization times and requires less control effort, from a statistical standpoint. Due to space constraints, in this letter, we limit the discussion to the attitude control problem; however, a position control scheme of the type presented in [4] can be straightforwardly integrated with the presented method for attitude control.

#### Notation-

- 1) Lowercase symbols represent scalars, e.g.,  $p$ ; bold lowercase symbols denote vectors, e.g.,  $\mathbf{p}$ ; bold uppercase symbols denote matrices, e.g.,  $\mathbf{P}$ ; and bold crossed lowercase symbols denote quaternions, e.g.,  $\mathbf{p}$ .
- 2) The set of unit vectors is denoted by  $\mathcal{S}^2$ . The special orthogonal group in the three-dimensional space is denoted by  $\mathcal{SO}(3)$ .
- 3) The sets of reals and positive reals are denoted by  $\mathbb{R}$  and  $\mathbb{R}_{>0}$ , respectively. The set of integers is denoted by  $\mathbb{Z}$ .
- 4) The symbols  $\times$  and  $\otimes$  respectively denote the cross-product of two vectors and the multiplication between two quaternions.
- 5) Throughout the rest of the paper, we use the notion of extended class  $\mathcal{K}_\infty$  function as defined in [19].

## II. BACKGROUND

We first describe the dynamics of a rigid body rotating in the 3D space. As shown in Fig. 1,  $\mathcal{B} = \{\mathbf{b}_1, \mathbf{b}_2, \mathbf{b}_3\}$  denotes the body-fixed frame of reference, with its origin coinciding with the body's *center of mass* (CoM), used for kinematic description and dynamic analysis. Consistent with this definition,  $\mathcal{I} = \{\mathbf{i}_1, \mathbf{i}_2, \mathbf{i}_3\}$  denotes the inertial frame of reference, fixed to the planet, used for formulation and analysis. As discussed in [4], [5], using quaternions and Euler's second law, the open-loop rotational dynamics of the system can be described according to

$$\dot{\mathbf{q}} = \frac{1}{2} \mathbf{q} \otimes \begin{bmatrix} 0 \\ \boldsymbol{\omega} \end{bmatrix}, \quad (1a)$$

$$\dot{\boldsymbol{\omega}} = \mathbf{J}^{-1} (\boldsymbol{\tau} - \boldsymbol{\omega} \times \mathbf{J} \boldsymbol{\omega}), \quad (1b)$$

in which  $\mathbf{q}$  is a unit quaternion that represents the orientation of  $\mathcal{B}$  relative to  $\mathcal{I}$ ;  $\boldsymbol{\omega}$  is the angular velocity of  $\mathcal{B}$  with respect to  $\mathcal{I}$ , written in  $\mathcal{B}$  coordinates;  $\mathbf{J}$  is the inertia matrix of the body, written in  $\mathcal{B}$  coordinates; and,  $\boldsymbol{\tau}$  is the torque applied to the system written in  $\mathcal{B}$  coordinates and, in closed loop, generated by a control law.

As specified by Euler's rotation theorem, any sequence of rotations of a rigid body in the 3D space is equivalent to a single rotation of amount  $\Theta$  about an axis  $\mathbf{u}$  that passes through the body's CoM. This information can be stored in the form of a unit quaternion as  $\mathbf{q} = [m \ \mathbf{n}^T]^T$ , where



**Fig. 1. Picture of the UAV used in the flight control experiments.** The Crazyflie 2.1 quadrotor and the definitions of the inertial frame of reference,  $\mathcal{I} = \{\mathbf{i}_1, \mathbf{i}_2, \mathbf{i}_3\}$ , fixed to the planet and the body-fixed frame of reference,  $\mathcal{B} = \{\mathbf{b}_1, \mathbf{b}_2, \mathbf{b}_3\}$  (shifted for clarity), whose origin is attached to the center of mass of the robot.

$m = \cos \frac{\Theta}{2}$  and  $\mathbf{n} = \mathbf{u} \sin \frac{\Theta}{2}$ . In the case specified by (1a),  $\Theta$  is the amount that the modeled body must be rotated about  $\mathbf{u}$  to reach the attitude of  $\mathcal{B}$  starting from  $\mathcal{I}$ . Accordingly, the instantaneous AEQ is given by  $\mathbf{q}_e = \mathbf{q}^{-1} \otimes \mathbf{q}_d = [m_e \ \mathbf{n}_e^T]^T$ , with  $m_e = \cos \frac{\Theta_e}{2}$  and  $\mathbf{n}_e = \mathbf{u}_e \sin \frac{\Theta_e}{2}$ , where  $\Theta_e$  is the amount that  $\mathcal{B}$  must be rotated about the attitude-error Euler axis,  $\mathbf{u}_e$ , to reach the orientation of the desired body-fixed frame,  $\mathcal{B}_d$ ; and,  $\mathbf{q}_d$  is a unit quaternion that represents the attitude of  $\mathcal{B}_d$  relative to  $\mathcal{I}$ . In practice,  $\mathbf{q}_d$  is either defined by a user, as described in Section IV, or generated by a position-control scheme, as explained in [4]. For the purpose of real-time implementation, the control algorithm must compute the desired angular-velocity quaternion of the rotational system, written in  $\mathcal{B}_d$  coordinates, according to

$$\begin{bmatrix} 0 \\ \hat{\boldsymbol{\omega}}_d \end{bmatrix} = 2\mathbf{q}_d^{-1} \otimes \dot{\mathbf{q}}_d. \quad (2)$$

Next, to obtain the desired angular velocity of the robot in  $\mathcal{B}$  coordinates, we use the transformation  $\boldsymbol{\omega}_d = \mathbf{S}^T \mathbf{S}_d \hat{\boldsymbol{\omega}}_d$ , where  $\mathbf{S}_d$  transforms vectors from  $\mathcal{B}_d$  to  $\mathcal{I}$  coordinates and  $\mathbf{S}^T$  transforms vectors from  $\mathcal{I}$  to  $\mathcal{B}$  coordinates. Then, the control law computes the torque input according to

$$\boldsymbol{\tau}_b = \mathbf{J} (k_q \mathbf{n}_e + k_\omega \boldsymbol{\omega}_e + \dot{\boldsymbol{\omega}}_d) + \boldsymbol{\omega} \times \mathbf{J} \boldsymbol{\omega}, \quad (3)$$

where  $k_q$  and  $k_\omega$  are scalar positive controller gains;  $\boldsymbol{\omega}_e = \boldsymbol{\omega}_d - \boldsymbol{\omega}$  is the angular-velocity tracking error;  $\mathbf{J} \dot{\boldsymbol{\omega}}_d$  is a feedforward term that cancels the left-hand side of (1b) and is included aiming to provide faster tracking performance; and,  $\boldsymbol{\omega} \times \mathbf{J} \boldsymbol{\omega}$  is a feedback-linearization term that cancels the nonlinearity present in (1b).

As discussed in [4], the CL rotational dynamics obtained by substituting the *right-hand side* (RHS) of (3) into (1b) exhibit two equilibria corresponding to the same kinematic condition but with different stability properties—one asymptotically stable and another unstable. It is straightforward to see that, at both fixed points,  $\mathbf{n}_e = \mathbf{0}$ . Therefore, if the state of the CL system were to be exactly at the unstable equilibrium point, the control torque specified by (3) would not compel the controlled rotational system to execute a  $2\pi$ -rad rotation and converge to the stable equilibrium point, thus preventing global asymptotic stability in  $\mathcal{SO}(3)$ . However, in any real-life application, any deviation from the unstable fixed point would make  $\mathbf{n}_e \neq \mathbf{0}$  and, therefore, for all practical purposes, we can confidently assume that the torque generated according to (3) forces the CL system's state to converge to the stable equilibrium point. Furthermore, since  $\mathbf{n}_e$  is scaled by the factor  $\sin \frac{\Theta_e}{2}$ ,

the first term in (3) does not provide the maximum allowable control effort when the controlled rotational system is at the farthest orientation from the stable CL equilibrium AEQ. In fact, this term reaches its minimum value at the unstable CL equilibrium AEQ, where  $\sin(2\pi/2) = 0$ ; its maximum at  $\sin(\pi/2) = 1$ ; and, its minimum again at the stable CL equilibrium AEQ, where  $\sin(0/2) = 0$ . These observations contradict the expected behavior of the proportional action of a feedback controller. We address this issue in the next section by proposing a new generalized axis-angle attitude law for controlling rotational systems in the 3D space.

### III. GENERALIZED AXIS-ANGLE ATTITUDE CONTROL

#### A. A New Class of Control Laws

Let  $\gamma : \mathbb{R} \mapsto \mathbb{R}$  be an extended  $\mathcal{K}_\infty$  function. Then, for a system whose dynamics evolve on  $SO(3)$ , the rotational errors to be minimized can be represented as

$$\alpha_e = \gamma(\Theta_e) \mathbf{u}_e \quad \text{and} \quad \omega_e, \quad (4)$$

where  $\alpha_e$  is a *scaled Euler axis* (SEA) aligned with  $\mathbf{u}_e$ , whose magnitude—measured by any vector norm—scales with the value of  $\Theta_e$ . Without loss of coverage of  $SO(3)$ ,  $\Theta_e$  can be restricted to any half-open interval spanning  $2\pi$ . In addition, given a selected interval, there exists a unique axis-angle pair representing any geometrically nontrivial attitude error; namely,  $\Theta_e \neq 2\pi k, \forall k \in \mathbb{Z}$ . When the attitude error is trivial, the corresponding rotation axis is not uniquely defined and can take any value in  $\mathcal{S}^2$ . Note, however, that  $\alpha_e$  is still well defined at  $\Theta_e = 0$ . For any nontrivial case, the selected domain for  $\Theta_e$  yields a  $\{\mathbf{u}_e, \Theta_e\}$  pair that defines one of two geometrically unique and opposite physical rotations. To deal with this rotational ambiguity, at initial time  $t_0$ , the direction of  $\mathbf{u}_e$  is selected to minimize a cost two-valued function over the interval  $\Theta_e \in [0, 2\pi)$ , as described in [1]. Thus, using the rotational errors specified by (4), we define the proposed generic control law as

$$\tau_\gamma = \mathbf{J} (k_\alpha \alpha_e + k_\delta \dot{\alpha}_e + k_\omega \omega_e + \dot{\omega}_d) + \omega \times \mathbf{J} \omega, \quad (5)$$

in which  $k_\alpha$ ,  $k_\delta$ , and  $k_\omega \in \mathbb{R}_{>0}$ . Then, from simple substitution of (4) into (5), we obtain that

$$\begin{aligned} \tau_\gamma = \mathbf{J} [k_\alpha \gamma(\Theta_e) \mathbf{u}_e + k_\delta \gamma(\Theta_e) \dot{\mathbf{u}}_e + k_\delta \dot{\gamma}(\Theta_e) \mathbf{u}_e \\ + k_\omega \omega_e + \dot{\omega}_d] + \omega \times \mathbf{J} \omega. \end{aligned} \quad (6)$$

#### B. Closed-Loop Dynamics & Equilibrium Points

It is straightforward to see that for the control input defined by (6), the CL rotational-error dynamics can be written as

$$\dot{\mathbf{q}}_e = \frac{1}{2} \begin{bmatrix} 0 \\ \omega_e \end{bmatrix} \otimes \mathbf{q}_e, \quad (7a)$$

$$\begin{aligned} \dot{\omega}_e = -k_\alpha \gamma(\Theta_e) \mathbf{u}_e - k_\delta \left[ \gamma(\Theta_e) \dot{\mathbf{u}}_e + \frac{\partial \gamma}{\partial \Theta_e} (\mathbf{u}_e^T \omega_e) \mathbf{u}_e \right] \\ - k_\omega \omega_e. \end{aligned} \quad (7b)$$

Also, it can be shown that  $\dot{\Theta}_e = \mathbf{u}_e^T \omega_e$ . Next, to find the equilibrium point(s) of the system specified by (7a)–(7b), we

solve for

$$\frac{1}{2} \mathbf{n}_e^T \omega_e = 0, \quad (8a)$$

$$-\frac{1}{2} (\mathbf{n}_e \times \omega_e - m_e \omega_e) = \mathbf{0}_{3 \times 1}, \quad (8b)$$

$$-k_\alpha \gamma(\Theta_e) \mathbf{u}_e - k_\delta \gamma(\Theta_e) \dot{\mathbf{u}}_e - k_\omega \omega_e = \mathbf{0}_{3 \times 1}. \quad (8c)$$

For (8b) to be satisfied, both terms inside the parenthesis must be zero because they are orthogonal. For both these terms to be zero, one of the following propositions must hold: (i)  $\mathbf{n}_e \parallel \omega_e$  and  $m_e = 0$ ; (ii)  $\omega_e = \mathbf{0}$ ; (iii)  $\mathbf{n}_e = \omega_e = \mathbf{0}$ . Also, for (8a) to be satisfied, either (ii) or (iii) is true,  $\mathbf{n}_e = \mathbf{0}$ , or  $\mathbf{n}_e \perp \omega_e$ . Since  $\mathbf{n}_e$  and  $\omega_e$  cannot simultaneously be orthogonal and parallel, the only viable option is either (ii) or (iii). The fulfillment of either (ii) or (iii) requires that the solution to (8a)–(8c) satisfies  $\omega_e^* = \mathbf{0}$ . Since  $\mathbf{u}_e$  is a unit vector evolving on  $\mathcal{S}^2$ , it follows that  $\mathbf{u}_e \perp \dot{\mathbf{u}}_e$  and, therefore, for (8c) to be satisfied,  $\gamma(\Theta_e) = 0$ . Last, recalling that  $\gamma(\Theta_e)$  is an extended  $\mathcal{K}_\infty$  function and, therefore,  $\gamma(0) = 0$ , we conclude that  $\Theta_e^* = 0$ .

It is important to note that for the law specified by (6), we selected  $\gamma(\Theta_e)$  to be an extended  $\mathcal{K}_\infty$  function in order to enforce the existence of a unique zero for  $\gamma(\Theta_e)$  and a unique equilibrium point for the CL dynamics given by (7a)–(7b), over the selected range of  $\Theta_e$ . In summary, the CL dynamics resulting from using the control input specified by (6) exhibit a unique equilibrium point, given by the quaternion-vector pair  $\mathbf{q}_e^* = [1 \ 0 \ 0 \ 0]^T$  and  $\omega_e^* = \mathbf{0}$ . This result does not contradict the topological obstruction discussed in [17] and references therein, according to which every continuous time-invariant CL vector field on  $SO(3)$  must exhibit more than one equilibrium point because, for the selected function  $\gamma(\cdot)$  and range for  $\Theta_e$ , the term  $\gamma(\Theta_e) \mathbf{u}_e$  is discontinuous at  $\Theta_e = 2\pi$  rad. As a consequence, the resulting CL dynamics specified by (7a)–(7b) are also discontinuous, which forces the existence of a unique fixed point, similarly to the cases presented in [8] and references therein. Because of the imposed discontinuity on the CL dynamics, to analyze the system of differential equations given by (7a)–(7b), we use Carathéodory's concept of solution as stated in Definition 2.1 of [20].

#### C. Stability Analysis

**Theorem 1.** *Let the attitude and angular-velocity references,  $\mathbf{q}_d$  and  $\omega_d$ , be smooth and bounded functions of time. Also, let the real controller gains satisfy  $k_\delta, k_\omega > 0$ , and  $k_\alpha > \frac{k_\delta k_\omega}{4}$ . Then, the fixed point  $\{\Theta_e^*, \omega_e^*\}$  of the CL state-space rotational dynamics specified by (7a) and (7b) is globally asymptotically stable.*

*Proof.* Let a candidate Lyapunov function be given by

$$\begin{aligned} V = \begin{bmatrix} \gamma(\Theta_e) \mathbf{u}_e^T & \omega_e^T \end{bmatrix} \begin{bmatrix} \frac{k_\delta^2}{2k_\alpha} & \frac{k_\delta}{2k_\alpha} \\ \frac{k_\delta}{2k_\alpha} & \frac{1}{2k_\alpha} \end{bmatrix} \begin{bmatrix} \gamma(\Theta_e) \mathbf{u}_e \\ \omega_e \end{bmatrix} \\ + \int_0^{\Theta_e} \gamma(\phi) d\phi. \end{aligned} \quad (9)$$

It is straightforward to show that the eigenvalues of the matrix in the quadratic term of (9) are

$$\lambda_1 = 0 \quad \text{and} \quad \lambda_2 = \frac{k_\delta^2 + 1}{2k_\alpha}. \quad (10)$$

Therefore, the quadratic term in (9) is positive semidefinite and  $V$  is positive definite because the second term is positive definite as long as  $\gamma(\cdot)$  exists strictly in the first and third quadrants, which is true for any extended  $\mathcal{K}_\infty$  function. This is a sufficient but not a necessary condition for positive definiteness. To continue, we expand  $V$  as

$$V = \frac{k_\delta^2}{2k_\alpha} \gamma^2(\Theta_e) + \frac{k_\delta}{k_\alpha} \gamma(\Theta_e) \mathbf{u}_e^T \boldsymbol{\omega}_e + \frac{1}{2k_\alpha} \boldsymbol{\omega}_e^T \boldsymbol{\omega}_e + \int_0^{\Theta_e} \gamma(\phi) d\phi, \quad (11)$$

and compute its time derivative, which yields

$$\dot{V} = \frac{k_\delta^2}{k_\alpha} \gamma(\Theta_e) \frac{\partial \gamma}{\partial \Theta_e} \dot{\Theta}_e + \frac{k_\delta}{k_\alpha} \left[ \frac{\partial \gamma}{\partial \Theta_e} \dot{\Theta}_e \mathbf{u}_e^T \boldsymbol{\omega}_e + \gamma(\Theta_e) \dot{\mathbf{u}}_e^T \boldsymbol{\omega}_e + \gamma(\Theta_e) \mathbf{u}_e^T \dot{\boldsymbol{\omega}}_e \right] + \frac{1}{k_\alpha} \boldsymbol{\omega}_e^T \dot{\boldsymbol{\omega}}_e + \gamma(\Theta_e) \dot{\Theta}_e, \quad (12)$$

which can be simplified by recalling that  $\dot{\Theta}_e = \mathbf{u}_e^T \boldsymbol{\omega}_e$ , noticing that  $\dot{\mathbf{u}}_e^T \mathbf{u}_e = 0$  because  $\mathbf{u}_e \in \mathcal{S}^2$ , and substituting (7b) into (12). Namely,

$$\begin{aligned} \dot{V} = & \frac{k_\delta^2}{k_\alpha} \gamma(\Theta_e) \frac{\partial \gamma}{\partial \Theta_e} \mathbf{u}_e^T \boldsymbol{\omega}_e \\ & + \frac{k_\delta}{k_\alpha} \left[ \frac{\partial \gamma}{\partial \Theta_e} \mathbf{u}_e^T \boldsymbol{\omega}_e \mathbf{u}_e^T \boldsymbol{\omega}_e + \gamma(\Theta_e) \dot{\mathbf{u}}_e^T \boldsymbol{\omega}_e - k_\alpha \gamma^2(\Theta_e) \right. \\ & \left. - k_\delta \gamma(\Theta_e) \frac{\partial \gamma}{\partial \Theta_e} (\mathbf{u}_e^T \boldsymbol{\omega}_e) - k_\omega \gamma(\Theta_e) \mathbf{u}_e^T \boldsymbol{\omega}_e \right] \\ & + \frac{1}{k_\alpha} \boldsymbol{\omega}_e^T \left[ -k_\alpha \gamma(\Theta_e) \mathbf{u}_e - k_\delta \left( \gamma(\Theta_e) \dot{\mathbf{u}}_e \right. \right. \\ & \left. \left. + \frac{\partial \gamma}{\partial \Theta_e} (\mathbf{u}_e^T \boldsymbol{\omega}_e) \mathbf{u}_e \right) - k_\omega \boldsymbol{\omega}_e \right] + \gamma(\Theta_e) \mathbf{u}_e^T \boldsymbol{\omega}_e. \end{aligned} \quad (13)$$

Thus, after canceling out the terms with equal magnitudes and opposite signs, we obtain

$$\begin{aligned} \dot{V} = & -k_\delta \gamma^2(\Theta_e) - \frac{k_\delta k_\omega}{k_\alpha} \gamma(\Theta_e) \mathbf{u}_e^T \boldsymbol{\omega}_e - \frac{k_\omega}{k_\alpha} \boldsymbol{\omega}_e^T \boldsymbol{\omega}_e \\ = & -[\gamma(\Theta_e) \mathbf{u}_e^T \quad \boldsymbol{\omega}_e^T] \mathbf{W} \begin{bmatrix} \gamma(\Theta_e) \mathbf{u}_e \\ \boldsymbol{\omega}_e \end{bmatrix}, \end{aligned} \quad (14)$$

where

$$\mathbf{W} = \begin{bmatrix} k_\delta & \frac{k_\delta k_\omega}{2k_\alpha} \\ \frac{k_\delta k_\omega}{2k_\alpha} & \frac{k_\omega}{k_\alpha} \end{bmatrix}, \quad (15)$$

which can be made positive definite by selecting

$$\{k_\delta, k_\omega\} > 0 \quad \text{and} \quad k_\alpha > \frac{k_\delta k_\omega}{4}, \quad (16)$$

thus also enforcing that  $\dot{V}(t) < 0$ . Last, by noticing that  $V$ , as specified by (9), is radially unbounded, we conclude that the unique fixed point of the CL dynamics given by (7a)–(7b),  $\{\Theta_e^*, \boldsymbol{\omega}_e^*\}$ , is globally asymptotically stable.  $\square$

A robustness analysis of the proposed control law is outside the scope of this letter; however, this task can be performed using the Lyapunov-based methods presented in [21].

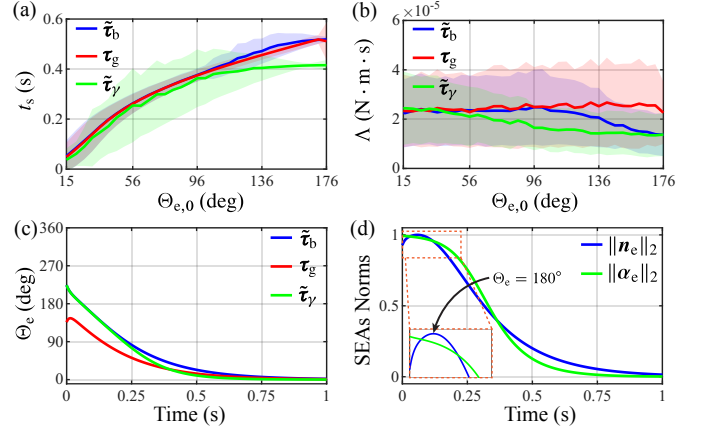


**Fig. 2. Numerical results with Crazyflie 2.1 parameters using quaternion-based, geometric, and axis-angle control laws.** (a) Mean and SD of the stabilization time over different initial rotation errors. (b) Mean and SD of the control effort variation over different initial rotation errors. (c) Time evolution of the rotation error associated with the attitude-error Euler axis. (d) Time evolution of the SEAs magnitudes for the quaternion-based and proposed axis-angle law.

#### D. Discussion

There exist infinitely many valid choices of  $\gamma(\cdot)$  functions; some superior to the rest. For example, a sigmoid function is an extended class  $\mathcal{K}_\infty$  function that provides tunable saturation while maintaining linearity near the equilibrium. Namely,

$$\gamma(\Theta_e) = \Theta_{\max} \frac{1 - e^{-\xi \frac{\Theta_e}{\Theta_{\max}}}}{1 + e^{-\xi \frac{\Theta_e}{\Theta_{\max}}}}, \quad (17)$$

where  $\Theta_{\max}$  and  $\xi$  are design parameters. In this context,  $\Theta_{\max}$  is the angle at which the maximum magnitude of the actuation torque occurs and  $\xi$  determines the rate at which the magnitude of  $\gamma(\Theta_e)$  changes with respect to  $\Theta_e$ . Taking the partial derivative of (17) with respect to  $\Theta_e$  yields

$$\frac{\partial \gamma}{\partial \Theta_e} = \frac{2\xi e^{-\xi \frac{\Theta_e}{\Theta_{\max}}}}{\left(1 + e^{-\xi \frac{\Theta_e}{\Theta_{\max}}}\right)^2}, \quad (18)$$

which provides insights and can be used to guide the process of controller synthesis. In particular, the slope at the origin has the form  $\frac{\partial \gamma}{\partial \Theta_e}(0) = \frac{\xi}{2}$ , in which  $\xi$  can be tuned taking into consideration, for example, actuator limitations and control objectives.

## IV. SIMULATION AND EXPERIMENTAL RESULTS

### A. Numerical Simulations

To systematically assess the functionality and performance of the proposed generalized control law, we compared a controller synthesized using this new approach with two benchmark schemes through numerical simulations. The first scheme used for comparison uses the quaternion-based attitude control law specified by (3),  $\tau_b$ ; the second is the high-performance geometric method presented in [12], whose corresponding attitude control law here we denote by  $\tau_g$ . We implemented and ran the simulations in Simulink 25.2 (MATLAB R2025b) using the Dormand-Prince algorithm with a fixed step of  $10^{-4}$  s. The open-loop dynamical model specified by (1a)–(1b) was incorporated into the simulations with the parameters of

the Crazyflie 2.1 platform—shown in Fig. 1—and empirically selected controller gains that satisfy the stability conditions for the three compared control laws. Specifically, we selected  $\mathbf{J} = \text{diag}\{16.6, 16.7, 29.3\} \cdot 10^{-6} \text{ kg} \cdot \text{m}^2$ ,  $k_q = 10^3 \text{ N} \cdot \text{m}$ , and  $k_\omega = 10^2 \text{ N} \cdot \text{m} \cdot \text{s}$  for  $\tau_b$  specified by (3). For  $\tau_g$  specified by (5), we selected  $k_\alpha = 10^3 \text{ N} \cdot \text{m}$ ,  $k_\omega = 10^2 \text{ N} \cdot \text{m} \cdot \text{s}$ , and  $k_\delta = 10 \text{ N} \cdot \text{m} \cdot \text{s}$  with  $\gamma(\Theta_e)$  defined by (17). For  $\gamma(\Theta_e)$ , we used  $\Theta_{\max} = 1 \text{ rad}$  and  $\xi = 1.5$ , which were chosen considering the actuator characteristics of the experimental platform. The controller gains for  $\tau_g$  were specified aiming to ensure an objective comparison. For consistency with previous published results, we implemented both  $\tau_g$  and  $\tau_b$  in combination with the *model predictive selection* (MPS) algorithm presented in [1], according to which the initial direction of  $\mathbf{u}_e$ , encoded by  $\sigma \in \{-1, +1\}$ , minimizes

$$\Gamma(\sigma, t) = \int_t^{t+t_h} [\tau^T(\sigma, \zeta) \mathbf{R} \tau(\sigma, \zeta) + \mathbf{n}_e^T(\zeta) \mathbf{Q} \mathbf{n}_e(\zeta)] d\zeta, \quad (19)$$

where  $t_h = 0.2 \text{ s}$ ;  $\mathbf{R} = \mathbf{I}$ ; and,  $\mathbf{Q} = 10^{-6} \cdot \mathbf{I}$ . In the simulations,  $\tau \in \{\tilde{\tau}_b(\sigma), \tilde{\tau}_g(\sigma)\}$ , with  $\tilde{\tau}_b(\sigma)$  defined as in [1] and

$$\tilde{\tau}_g(\sigma) = \mathbf{J} [k_\alpha \alpha_e(\sigma) + k_\delta \dot{\alpha}_e(\sigma) + k_\omega \omega_e + \dot{\omega}_d] + \omega \times \mathbf{J} \omega, \quad (20)$$

in which  $\alpha_e(\sigma) = \sigma \gamma(\Phi_e) \mathbf{u}_e$  and  $\Phi_e = (1 - \sigma) \pi + \sigma \Theta_e$ . Note that for  $\sigma = +1$ ,  $\Phi_e = \Theta_e$ , and for  $\sigma = -1$ ,  $\Phi_e = 2\pi - \Theta_e$ .

In total, we performed 10908 simulations of high-speed tumble-recovery maneuvers, in which the control objective was to stabilize the orientation of the UAV from an initial state with arbitrary attitude and angular velocity. Consistent with stabilization, for each simulation, the desired state was set to  $\mathbf{q}_d = [1 \ 0 \ 0 \ 0]^T$  and  $\omega_d = \mathbf{0} \text{ rad} \cdot \text{s}^{-1}$ . The directions of the initial Euler axes of rotation,  $\mathbf{u}_0 = \mathbf{u}(t_0)$ , were randomly selected from the unit sphere using a uniform distribution, and the initial rotations about  $\mathbf{u}_0$ ,  $\Theta_0 = \Theta(t_0)$ , were taken from the set  $[1 : 180]^\circ$  in steps of  $5^\circ$ . For each  $\Theta_0$ , we varied the initial angular velocity,  $\omega_0$ , from  $-30 \cdot \mathbf{u}_0$  to  $30 \cdot \mathbf{u}_0 \text{ rad} \cdot \text{s}^{-1}$  with the magnitude incremented in steps of  $0.6 \text{ rad} \cdot \text{s}^{-1}$ . For each simulation corresponding to a  $\Theta_0$  value, we computed the mean and *standard deviation* (SD) of the stabilization time,  $t_s$ —defined as the time it takes for  $\Theta_e$  to reach a value lower than  $15^\circ$ —across the 101 different values of  $\omega_0$ . Fig. 2(a) shows how the mean (solid line) and SD (reduced-opacity band) of the stabilization time vary as functions of the initial rotation error,  $\Theta_{e,0}$ , for the three simulated controllers. As seen, the means of the stabilization time obtained with the three controllers are similar for small values of  $\Theta_{e,0}$ ; however, for larger values of  $\Theta_{e,0}$  the means of the stabilization time obtained with  $\tau_g$  are notably smaller, even though  $\tau_g$  produces a better performance in some cases—as evidenced by the SD data. Fig. 2(b) shows the mean and SD of the control effort—defined as  $\Lambda = \int_0^1 \|\tau(t)\|_2 dt$ , with  $\tau \in \{\tilde{\tau}_b, \tau_g, \tilde{\tau}_g\}$ —as functions of  $\Theta_{e,0}$ , for the same simulations corresponding to Fig. 2(a). Although the means of the control effort obtained with the three controllers are similar for small values of  $\Theta_{e,0}$ , the values of  $\Lambda$  corresponding to  $\tau_b$  and  $\tau_g$  decrease as  $\Theta_{e,0}$  increases. Remarkably, the proposed controller consistently requires less control effort while achieving a lower mean stabilization time compared to the two benchmark controllers.

Fig. 2(c) shows the time evolution of  $\Theta_e$  corresponding to the three simulated control laws, with an initial condition of

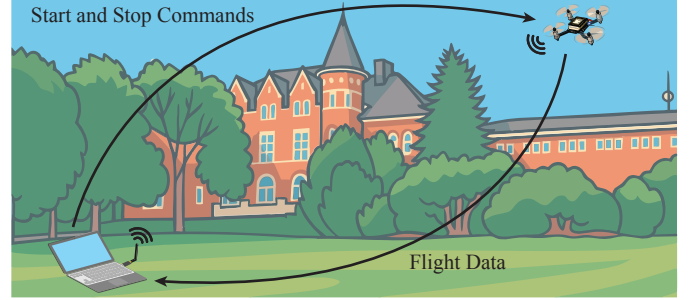


**Fig. 3. Experimental setup used during the flight tests.** The attitude flight control experiments were run outdoors using a ground computer equipped with the Crazyradio 2.0 to communicate with the Crazyflie 2.1.

$\Theta_0 = 136^\circ$  and  $\omega_0 = 30 \cdot \mathbf{u}_0 \text{ rad} \cdot \text{s}^{-1}$ . This initial state corresponds to a kinematic condition in which the direction of the system's initial angular velocity is opposite to that of the shorter rotational path required to eliminate the attitude error. As seen, the controller based on  $\tilde{\tau}_g$  achieves a stabilization time of 0.45 s whereas the benchmark controllers—with laws  $\tilde{\tau}_b$  and  $\tau_g$ —achieve stabilization times of 0.58 and 0.49 s, respectively. It is important to note that the initial rotation error for the  $\tilde{\tau}_g$  and  $\tilde{\tau}_b$  cases is  $224^\circ$ , which means that these two laws applied the control torque in the direction of the longer rotational path required to eliminate the attitude error. Fig. 2(d) shows the magnitudes of the corresponding SEAs,  $\|\mathbf{n}_e\|_2$  and  $\|\alpha_e\|_2$ . As seen,  $\|\mathbf{n}_e\|_2$  increases as the control error decreases down to  $\Theta_e = 180^\circ$  and starts decreasing after passing through that point (see inset), which highlights the characteristic behavior of quaternion-based controllers. In contrast,  $\|\alpha_e\|_2$  decreases with  $\Theta_e$ , as intended by design.

## B. Real-Time Flight Experiments

To assess and demonstrate the suitability and performance of the proposed axis–angle control approach, we performed real-time flight experiments using the same three controllers described in Section IV-A. As depicted in Fig. 3, the flight tests were conducted outdoors, using a ground computer—equipped with the Crazyradio 2.0 2.4-GHz USB radio transceiver—to send initialization and stop commands, and collect the flight and control data at a rate of 100 Hz. During each test, the UAV was required to execute a high-speed tumble-recovery maneuver after a throw launch. A representative experiment consists of two stages. In the first stage, the tested UAV is thrown into the air with an arbitrary high angular velocity, while the controller and propellers remain inactive; in the second stage, the controller and propellers are activated. Throughout a maneuver, the flier operates entirely autonomously, using only onboard sensing and computation, with the tested attitude controller running at 500 Hz.

Fig. 4(a) presents the time evolution of  $\Theta_e$  for different experiments with similar initial conditions, using the three tested control laws. As seen, the stabilization times corresponding to  $\tilde{\tau}_b$ ,  $\tau_g$ , and  $\tilde{\tau}_g$  are of 0.57, 0.50, and 0.48 s, respectively. Interestingly, the corresponding values of  $\Lambda$  for the  $\tau_g$  and  $\tilde{\tau}_g$  laws are  $1.76 \cdot 10^{-4}$  and  $4.56 \cdot 10^{-5}$ , which indicates that the proposed method achieved a lower stabilization time using only 25% of the control effort measured for the geometric-control case. Fig. 4(b) presents the time evolutions

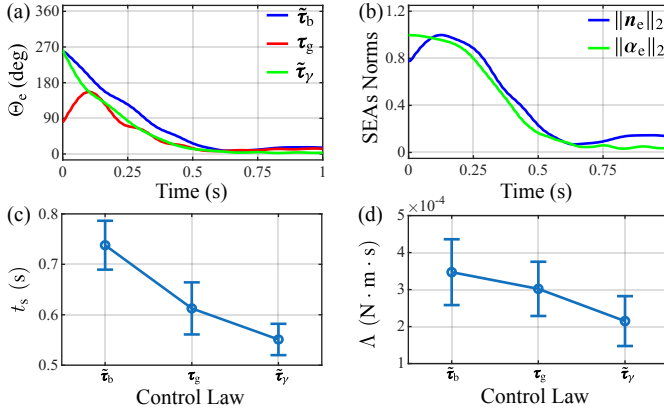


**Fig. 4. Experimental results.** (a) Rotation errors corresponding to three tests employing  $\tilde{\tau}_b$ ,  $\tau_g$ , and  $\tilde{\tau}_y$ . (b) Magnitudes of the SEAs  $\|\mathbf{n}_e\|_2$  and  $\|\boldsymbol{\alpha}_e\|_2$  corresponding to  $\tilde{\tau}_b$  and  $\tilde{\tau}_y$ , respectively. (c) Comparison of mean (circle) and SEM (vertical bars) of the stabilization times using  $\tilde{\tau}_b$ ,  $\tau_g$ , and  $\tilde{\tau}_y$  over 30 experiments. (d) Comparison of mean and SEM of the control effort using  $\tilde{\tau}_b$ ,  $\tau_g$ , and  $\tilde{\tau}_y$  over 30 experiments.

of the 2-norms of the SEA vectors  $\|\mathbf{n}_e\|_2$  and  $\|\boldsymbol{\alpha}_e\|_2$ . Similarly to the simulation cases discussed in Section IV-A, it can be observed that  $\|\mathbf{n}_e\|_2$  increases as  $\Theta_e$  decreases down to  $180^\circ$ , and decreases after passing through this point. In contrast, over the entire range of operation,  $\|\boldsymbol{\alpha}_e\|_2$  decreases and increases with  $\Theta_e$ , as intended by design. Experiments of this type can be viewed in the video available as a Supplemental Item.

In Fig. 4(c), each data point indicates the mean and *standard error of the mean* (SEM) of the stabilization times corresponding to 30 back-to-back experiments performed using each of the three control laws compared in this letter. The means of the stabilization times corresponding to  $\tilde{\tau}_b$ ,  $\tau_g$ , and  $\tilde{\tau}_y$  are 0.74, 0.61, and 0.55 s, respectively. In Fig. 4(d), each data point indicates the the mean and SEM of the control effort,  $\Lambda$ , corresponding to the same experiments in Fig. 4(c). Specifically, the means of  $\Lambda$  corresponding to  $\tilde{\tau}_b$ ,  $\tau_g$ , and  $\tilde{\tau}_y$  are  $3.47 \cdot 10^{-4}$ ,  $3.02 \cdot 10^{-4}$ , and  $2.15 \cdot 10^{-4} \text{ N} \cdot \text{m} \cdot \text{s}$ , respectively. Although the differences between these values are not substantial, the experimental data provide compelling evidence of the suitability and superior performance of the proposed approach; particularly, under nonideal conditions due to the presence of actuator saturation, model uncertainty, and disturbances. We inferred that these nonideal conditions also explain the discrepancies between the simulated and experimental  $\Lambda$  values. Last, it is important to mention that the large variability in the experimental data is expected due to the random nature of tumble-recovery experiments.

## V. CONCLUSION

We introduced a new class of axis-angle attitude control laws that provide substantial design flexibility with guaranteed closed-loop stability while ensuring a greater proportional control effort the farther away the system's state is from the unique stable fixed AEQ of the CL dynamics. This characteristic is particularly useful when the proposed approach is used in combination with intelligent switching schemes. Evidence regarding functionality and high performance was provided in the form of data obtained through simulations and outdoor flight tests, during which we commanded a quadrotor to autonomously execute tumble-recovery maneuvers in the

air. The new method consistently achieved reduced stabilization times and required less control effort compared to the quaternion-based and geometric-control methods used as benchmarks.

## REFERENCES

- [1] F. M. F. R. Gonçalves, R. M. Bena, K. I. Matveev, and N. O. Pérez-Arcibia, "MPS: A New Method for Selecting the Stable Closed-Loop Equilibrium Attitude-Error Quaternion of a UAV During Flight," in *Proc. IEEE Int. Conf. Robot. Autom. (ICRA)*, Yokohama, Japan, May 2024, pp. 8363–8369.
- [2] F. M. F. R. Gonçalves, R. M. Bena, and N. O. Pérez-Arcibia, "Closed-Loop Stability of a Lyapunov-Based Switching Scheme for Energy-Efficient Torque-Input-Selection During Flight," in *Proc. IEEE Int. Conf. Robot. Biomim. (ROBIO)*, Bangkok, Thailand, Dec. 2024, pp. 1941–1947.
- [3] R. Schlanbusch, A. Loria, and P. J. Nicklasson, "On the stability and stabilization of quaternion equilibria of rigid bodies," *Automatica*, vol. 48, no. 12, pp. 3135–3141, 2012.
- [4] R. M. Bena, X.-T. Nguyen, X. Yang, A. A. Calderón, Y. Chen, and N. O. Pérez-Arcibia, "A Multiplatform Position Control Scheme for Flying Robotic Insects," *J. Intell. Robot. Syst.*, vol. 105, no. 1, May 2022, Art. no. 19.
- [5] R. M. Bena, X. Yang, A. A. Calderón, and N. O. Pérez-Arcibia, "High-Performance Six-DOF Flight Control of the Bee<sup>++</sup>: An Inclined-Stroke-Plane Approach," *IEEE Trans. Robot.*, vol. 39, no. 2, pp. 1668–1684, Apr. 2023.
- [6] C. G. Mayhew, R. G. Sanfelice, and A. R. Teel, "Robust Global Asymptotic Attitude Stabilization of a Rigid Body by Quaternion-Based Hybrid Feedback," in *Proc. IEEE Conf. Decis. Control (CDC)*, Chin. Control Conf. (CCC), Shanghai, China, Dec. 2009, pp. 2522–2527.
- [7] —, "On Quaternion-Based Attitude Control and the Unwinding Phenomenon," in *Proc. Amer. Control Conf. (ACC)*, San Francisco, CA, USA, Jun. 2011, pp. 299–304.
- [8] —, "Quaternion-Based Hybrid Control for Robust Global Attitude Tracking," *IEEE Trans. Autom. Control*, vol. 56, no. 11, pp. 2555–2566, Nov. 2011.
- [9] B. Pratama, A. Muis, A. Subiantoro, M. Djemai, and R. B. Atitallah, "Quadcopter Trajectory Tracking and Attitude Control Based on Euler Angle Limitation," in *Proc. 6th Int. Conf. Control Eng. Inf. Technol. (CETT)*, Istanbul, Turkey, Oct. 2018, Art. no. 8751819.
- [10] A. Mokhtari and A. Benallegue, "Dynamic Feedback Controller of Euler Angles and Wind Parameters Estimation for a Quadrotor Unmanned Aerial Vehicle," in *Proc. IEEE Int. Conf. Robot. Autom. (ICRA)*, New Orleans, LA, USA, Apr. 2004, pp. 2359–2366.
- [11] C. W. Kang and C. G. Park, "Euler Angle Based Attitude Estimation Avoiding the Singularity Problem," in *Proc. 18th IFAC World Cong. (IFAC'11)*, Milan, Italy, Aug. 2011, pp. 2096–2102.
- [12] T. Lee, "Geometric Tracking Control of the Attitude Dynamics of a Rigid Body on  $\text{SO}(3)$ ," in *Proc. Amer. Control Conf. (ACC)*, San Francisco, CA, USA, Jun. 2011, pp. 1200–1205.
- [13] —, "Geometric Control of Quadrotor UAVs Transporting a Cable-Suspended Rigid Body," *IEEE Trans. Control Syst. Technol.*, vol. 26, no. 1, pp. 255–264, Jan. 2018.
- [14] G. Wu and K. Sreenath, "Geometric Control of Multiple Quadrotors Transporting a Rigid-body Load," in *Proc. IEEE Conf. Decis. Control (CDC)*, Los Angeles, CA, USA, Dec. 2014, pp. 6141–6148.
- [15] J. Wei, S. Zhang, A. Adaldo, X. Hu, and K. H. Johansson, "Finite-time attitude synchronization with a discontinuous protocol," in *Proc. Int. Conf. Control Autom. (ICCA)*, Ohrid, Macedonia, Jul. 2017, pp. 192–197.
- [16] J. Thunberg, W. Song, E. Montijano, Y. Hong, and X. Hu, "Distributed attitude synchronization control of multi-agent systems with switching topologies," *Automatica*, vol. 50, no. 3, pp. 832–840, Mar. 2014.
- [17] N. A. Chaturvedi, A. K. Sanyal, and N. H. McClamroch, "Rigid-Body Attitude Control," *IEEE Control Syst. Mag.*, vol. 31, no. 3, pp. 30–51, Jun. 2011.
- [18] J. B. Kuipers, *Quaternions and Rotation Sequences: A Primer with Applications to Orbits, Aerospace and Virtual Reality*. Princeton, NJ, USA: Princeton University Press, 2002.
- [19] A. D. Ames, X. Xu, J. W. Frizzle, and P. Tabuada, "Control Barrier Function Based Quadratic Programs for Safety Critical Systems," *IEEE Trans. Autom. Control*, vol. 62, no. 8, pp. 3861–3876, Aug. 2017.
- [20] O. Hájek, "Discontinuous differential equations, I," *J. Differ. Equ.*, vol. 32, no. 2, pp. 149–170, May 1979.
- [21] H. K. Khalil, *Nonlinear Systems*. Upper Saddle River, NJ, USA: Prentice-Hall, 2002.